ROMO1 is essential for glucose coupling in the pancreatic β cell of male mice

Authors: Lisa Wells[1], Caterina Iorio[1], Andy Cheuk-Him Ng[1], Courtney Reeks[1], Siu-Pok Yee[2], Robert A. Screaton[1,3*].

Affiliations:

[1]Sunnybrook Research Institute, 2075 Bayview Avenue, Toronto, M4N 3M5, Canada.

[2]Department of Genetics and Developmental Biology, University of Connecticut Health Center, Farmington, Connecticut, USA, 06030.

[3]Department of Biochemistry, University of Toronto, Toronto, M5S 1A8, Canada.

*Corresponding Author.

Email: robert.screaton@sri.utoronto.ca

Phone: (416) 480-6100 X 5743

Word Count: 3959

Number of tables and figures: 4

Running title: ROMO1 is required for glucose coupling in male mice

Keywords: ROMO1, pancreatic β cell, islet, RNA interference (RNAi), mitochondria, Type 2 diabetes, spare respiratory capacity

Abstract

Reactive oxygen species modulator 1 (ROMO1) is a highly conserved inner mitochondrial membrane protein that senses ROS and regulates mitochondrial dynamics [1]. ROMO1 is required for mitochondrial fusion *in vitro*, and silencing ROMO1 increases sensitivity to cell death stimuli. How ROMO1 promotes mitochondrial fusion and its physiological role remain unclear. Here we show that ROMO1 is essential for embryonic development, as ROMO1-null mice die before embryonic day 8.5, earlier than GTPases OPA1 or MFN1/2 that catalyze mitochondrial membrane fusion. Knockout of ROMO1 in adult pancreatic β cells results in impaired glucose homeostasis in male mice due to an insulin secretion defect resulting from impaired glucose sensing. Mitochondria in ROMO1 β cell KO cells were swollen and fragmented, consistent with a role for ROMO1 in mitochondrial fusion *in vivo*. While basal respiration was normal in ROMO1β cell KO islets, spare respiratory capacity was lost. Taken together, our data indicate that ROMO1 is required for nutrient coupling in the β cell and point to a critical role for spare respiratory capacity in the maintenance of euglycemia in males.

Introduction

Mitochondria are the primary organelles of ATP production from nutrient stores and their integrity is central to cell survival. In the presence of oxygen, mitochondria harness electron reducing

equivalents derived from the tricarboxylic acid (TCA) cycle and fatty acid oxidation to fuel the electron transport chain and establish a proton gradient across the inner mitochondrial membrane (IMM) that drives ATP synthesis [2]. Mitochondria also participate in the synthesis and breakdown of macromolecules including glucose, fatty acids, nucleotides and amino acids, and serve as buffers for calcium ion [3,4]. Mitochondrial dysfunction is a characteristic of aging [5] and is thought to underlie numerous human diseases, including cardiovascular disease [6], atherosclerosis [7,8], neurodegeneration [9], as well as cancer and diabetes [10]. Mitochondrial dysfunction is most effectively monitored via functional assessment of mitochondrial oxidative capacity, and as they are critical sites for the generation and balancing of redox equivalents, by their production of reactive oxygen species (ROS) [11]. Accumulation of damaging ROS resulting from premature deposition of electrons on molecular oxygen is thought to drive mitochondrial dysfunction. ROS targets include mtDNA, proteins and membrane lipids, all of which lead to reduced respiratory capacity. The uncontrolled production of ROS can induce permeabilization of the OMM and the release of factors (cytochrome c, SMAC/Diablo) that activate the mitochondrial apoptotic cascade [12].

Reactive Oxygen Species Modulator 1 (ROMO1) is a highly conserved inner mitochondrial membrane (IMM) protein that has been reported to drive reactive oxygen species (ROS) production in cancer cells [13-16]. Furthermore, ROMO1 has been shown to govern the selective import of mitochondrial protein targets, including the protease YME1L [17], and demonstrates nonselective cation channel activity *in vitro* [18]. In a genome-wide RNAi screen to identify regulators of mitochondrial dynamics, we showed that ROMO1 is a redox protein required for OPA1 processing, and that silencing ROMO1 increases ROS, fragments the mitochondrial

network, and increases sensitivity to apoptotic stimuli [1]. In addition, U2OS cells lacking ROMO1 demonstrated a complete loss of spare respiratory capacity (SRC), which is a key feature of mitochondrial dysfunction under stress and aging. Here we generated mice lacking the ROMO1 gene to gain insight into the role of ROMO1 in SRC *in vivo*.

Research Design and Methods

Mice. All animal procedures were approved by the Animal Care Committee in Sunnybrook Research Institute, and experiments were carried out in accordance with the accepted guidelines. Animals were fed Irradiated 18% Protein Rodent Diet (Envigo Teklad Global #2918-12159M) *ad libitum*. In all animal experiments, no statistical method was used to predetermine sample size and the experiments were not randomized. The investigators were not blinded to allocation during experiments and outcome assessment.

Knockout mice. The targeting vector designed carrying loxP sites flanking *ROMO1* exon 3 (Figure 1A) was transfected into C57BL/6-129/SvEv ES cells by electroporation. Exon 3 encodes Ile45-Cys79 which is predicted to encode the 10-residue loop between the first and second TM domain and includes the TAA stop codon. The resulting recombined product is predicted to generate an out-of-frame mRNA subject to nonsense-mediated decay. G418-resistant colonies were screened by PCR. Targeted ES cells were injected into C57BL/6 blastocysts to create chimeric mice. To create the null ROMO1 allele, *Romo1*$^{loxP/loxP}$ mice (C57BL6/129sv background)

were mated to universal Cre (HPRT-Cre) mice to generate cohorts as follows: *Romo1*$^{loxP/loxP}$:HPRT-Cre^{+} and *Romo1*$^{loxP/+}$: HPRT-Cre^{+}, as well as appropriate controls lacking Cre. Genomic DNA was isolated using E.Z.N.A. Tissue DNA kit (Omega BIO-TSK D3396-02) using tail or ear clippings at 3 weeks of age, and PCR genotyping was performed with GoTaq polymerase (Promega M712). To detect the deletion of *Romo1* gene and the floxed-*Romo1* allele, the following primer sets were used: LoxgtF–5'TTACATTATCTGGCACGTCG and LoxgtR – 5' AGGCTAGTATCGAACTCAGG. The WT allele product = 299bp, floxed allele product= 394bp. To detect Cre, the following primers were used: Cre 26 – 5' CCTGGAAAATGCTTCTGTCCG; Cre 36 – 5' CAGGGTGTTATAAGCAATCCC. Internal control primers were Gabra12: 5'-CAATGGTAGGCTCACTCTGGGAGATG-3') and Gabra70 5'-AACACACACTGGCAGGACTGGCTAG-3', product = 300 bp.

ROMO1 adult β knockout (RABKO) mice: Mice carrying the ROMO1 floxed allele were bred with mice carrying a *Pdx1*-Cre-ER^{Tam} transgene, which in adult mice drives tamoxifen-inducible Cre expression only in the β cell. 8 week old mice were injected intraperitoneally with three injections of tamoxifen on alternating days at 5 mg/40g body weight [19].

Histology. After timed breeding and confirmation of vaginal plugs, embryos were isolated at E8.5-10.5. For whole-mount immunohistochemistry, embryos were fixed in 4% paraformaldehyde in PBS overnight at 4°C prior to imaging.

Blood Glucose measurements. Mice were fasted for 16 hours before sampling 30 ul of blood from the tail vein, then sampled again after 1 hour of refeeding with chow diet. Blood glucose levels were monitored using OneTouch Ultra Test Strips (AW07052001A).

Glucose Tolerance Test was performed as described (Sakamaki et al.). Briefly, mice were fasted for 16h prior to IP injection of 2 g/kg body weight glucose (SIGMA G7021) in PBS. Samples were taken at indicated times.

Insulin Tolerance Test. Mice were fasted for 4 hours. Freshly prepared Insulin (Humalog VL7510 DIN 02229704) was injected IP at 0.5 U/kg. 30 ul blood samples were taken at indicated times.

Plasma Insulin measurements. Mice were fasted for 16h. Blood samples from the lateral saphenous vein taken at indicated timepoints were transferred to heparinized capillary tubes (FisherBrand 22-260-950), clarified by centrifugation at 15,000xg for 3 minutes and stored at -80C prior to assay with the Ultra-Sensitive Mouse Insulin Kit (Crystal Chem 90080).

Arginine Tolerance Test. Mice were fasted for 16 hours. Freshly prepared L-Arginine (SIGMA, A8094) was injected at 1g/kg body weight and 75 ul blood was collected in capillary tubes at 0, 2, and 5 minutes post-injection.

Tissue isolation. Mice were euthanized, weighed, and pancreas perfused with collagenase (Sigma C7657-5G) [19]. Islets were handpicked under microscope and cultured in RPMI media (Life

Technologies, 11875-093) supplemented with 10% fetal calf serum (Wisent Bioproducts, 088150), 10 mM glucose and antibiotics at 37C overnight before use. Left and right cortex, and hypothalamus were collected and placed on ice and stored at -80C. 30 mg of each tissue was used for lysis with RIPA for western blot analysis.

GSIS: 10 size-matched islets per sample were starved in Krebs Ringer Buffer supplemented with 2.8 mM glucose for 2h, then treated with the indicated concentrations of glucose for 1h, followed by 45 mM KCl to evaluate depolarization-induced secretion [20]. Insulin content was determined by acid-EtOH extraction. Insulin levels were determined by HTRF (Cisbio) [19]. The insulin levels were normalized to DNA levels using the Quant-iT dsDNA Assay Kit (Life Technologies).

Cell Culture and Reagents. HEK293T and U2OS cells were obtained from ATCC and cultured in DMEM + 10% FCS + antibiotics in a humidified atmosphere with 5% CO_2. For plasmid transfection, HEK293T were transfected using PEI (Polysciences Inc).

Antibodies. MFN1 (1:1000), MFN2 (1:1000), VDAC1 (1:1000) were from Cell Signaling Technology, ERK2 (1:1000) and TOMM20 (1:1000) were from Santa Cruz, ROMO1 (1:2000) was from Origene, OPA1 (1:1000), SOD2 (1:2000) were from Abcam, and insulin and glucagon were from Dako. Insulin-647 conjugated antibody was from BD Biosciences.

RNA interference was performed as described [1].

SDS-PAGE and Western Blotting Tissue samples were homogenized in RIPA buffer (50 mM TRIS pH 7.5, 150 mM NaCl, 0.1% SDS, 1% NP-40, 12 mM sodium deoxycholate) with Halt Protease Inhibitor Cocktail (Thermo Scientific) and 50 mM PMSF added fresh. Secondary antibodies (3 uL IRDye 800CW Donkey anti-Rabbit IgG, 1.5 uL IRDye 680RD Donkey anti-Mouse IgG; LI-COR) were diluted in 3% milk in PBS containing 0.01% SDS and 0.04% Triton-X 100. Immunoblots were scanned with Odyssey CLx Imaging System and quantified with LI-COR Image Studio Acquisition Software. Western blotting to confirm ROMO1 KO was performed two weeks post-tamoxifen injection using 75 isolated islets per sample. Data presented are representative of at least two independent experiments.

Quantitative RT-PCR Assays were performed on a Mastercycler EP Realplex 2 (Eppendorf) using a QuantiTect SYBR green PCR kit (Qiagen). Relative gene expression was determined by ΔΔCT normalized to expression of 36b4 internal control. The following primer sets were used: mouse ROMO1 (5'-GCCTTGTACCTCGACTCTGC-3' and 5'-CCCCCAAGTCAGGTGTTCTA-3'), mouse NFS1 (5'-GCAGCTCACAACCCCATTGTG-3' and 5'-GGACTTCAGGACACCGCATC-3'), mouse 36b4 (5'-CCACGAAAATCTCCAGAGGCAC-3' and 5'-ATGATCAGCCCGAAGGAGAAGG-3').

Mitochondrial isolation: Liver tissue was homogenized with a Teflon pestle in mitochondrial assay solution on ice (70 mM sucrose, 220 mM mannitol, 10 mM KH_2PO_4, 5 mM $MgCl_2$, 2 mM HEPES, 1 mM EGTA, pH 7.4). Homogenate was centrifuged at 800g for 10 mins at 4C. Supernatant was collected and centrifuged at 8000g for 10 mins at 4°C twice. Mitochondrial pellets

were resuspended with mitochondrial assay solution and protein content determined by BCA assay (Thermo Scientific).

Mitochondrial stress test. Isolated mitochondria: 2 ug mitochondria from WT or ROMO1 liver ko mice were seeded per well of a XFe96 Seahorse cell culture microplate. Cells: U2OS cells were infected with lenti-shRNA targeting ROMO1 or non-silencing control on Seahorse XFe96 cell culture microplate on day 0 [1]. On day 3, cells were starved in 180 uL of Seahorse XF assay medium containing 1 mM glucose for 60 min, and oxygen consumption rate (OCR) was measured following treatment with stimuli as follows: 5 mM succinate, 5 mM glutamate, 2.5 mM malate, 5 mM pyruvate, 2 mM ADP, 2 uM oligomycin, 2 uM FCCP, 1 uM rotenone, 1 uM antimycin. B cells: Islets isolated from mice or from human donors were washed in PBS and dissociated with Accutase (1ml/1000 IEQ) for 3-5 min at 37˚C and triturated every 60 sec. Dissociated islet cells were seeded at a density of 40,000 cells/well in a XFe96 well Seahorse plate that was coated with poly(D)lysine. On day of assay, cells were treated as described for U2OS cells and OCR was measured with stimuli as follows: 2 uM oligomycin, 1 uM FCCP, 1 uM rotenone, 1 uM antimycin, and 0.5 mM TMPD/5 mM Ascorbate. Protein content was quantified by BCA assay (Thermo Scientific).

Proteinase K Assay. Mitochondria were treated without or with osmotic shock to rupture the outer membrane. Samples with treated with indicated amounts of proteinase K and Western blots performed on the non-digested pelleted material.

Electron Microscopy Islets from WT and RABKO mice were picked and fixed with 4% paraformaldehyde, 1% glutaraldehyde for 24 hr, then washed with 0.1 M phosphate buffer, pH 7.0 and post-fixed with 1% osmium tetroxide in 0.1 M phosphate buffer, pH 7.0, for 1 hr. Islets were washed with 0.1 M phosphate buffer, pH 7.0 then dehydrated in an ethanol series. Islets were infiltrated with Embed 812/Araldite resin and cured at 65°C for 48 hr. Resin blocks were trimmed, polished and 90 nm thin sections were sectioned with a Leica Reichert Ultracut E ultramicrotome and mounted on TEM grids. Thin sections were stained with 5% uranyl acetate and 5% lead citrate. Sections were imaged using Transmission Electron Microscopy (Thermo Scientific Talos L120C) using a LaB6 filament at 120kV. For each sample 20 grid squares were imaged at 3,400x and 13,500x magnification.

Immunohistochemistry Paraffin-embedded pancreatic sections were stained with insulin (DAKO, A0564),and glucagon (DAKO, A0565) antibodies as described [19]. For β cell mass determination, sections were stained with Insulin Ab (DAKO, A0564) and visualized with Vectastain ABC HRP Kit (Vector Labs, PK6100) and DAB solution kit (Vector Labs, SK4105). Slides were imaged at the Advanced Optical Microscopy Facility (AOMF), UHN Research. B cell area was determined using ImageScope software.

Statistical analyses. All studies were performed on at least three independent occasions. Results are reported as mean ± s.e.m. Statistical significance for all data was determined using two-tailed unpaired Student's *t*-test; p-values < 0.05 were considered significant. Significance in all figures is indicated as follows: * $p < 0.05$, ** $p < 0.01$, *** $p < 0.001$.

Results

To investigate the *in vivo* function of ROMO1, we generated complete and conditional mouse knockouts using a floxed ROMO1 allele (Fig. 1A). As the *Nfs1* gene is transcribed from the opposite strand in a genomic region that overlaps with exon 1 of ROMO1, we chose to target exon 3 with *loxP* sites (Figure 1A). We crossed *ROMO1*$^{+/fl}$ mice to mice carrying an *HPRT*-Cre transgene, consisting of Cre recombinase driven by promoter sequences from the HPRT gene that is involved in purine biosynthesis and is ubiquitously expressed. Following recombination, the predicted ROMO1 mRNA lacking exon 3 would generate an out of frame product and be subject to nonsense-mediated decay. To examine the effect of complete loss of ROMO1, we analyzed the genotype of 69 progeny from crosses of heterozygous mice. *ROMO1* heterozygous mice express a partially reduced level of ROMO1 protein (not shown) and are viable. None of the progeny were homozygous for deletion of ROMO1 (Fig. 1 C) indicating that homozygous deletion of ROMO1 leads to embryonic lethality. Dissection of embryos from pregnant female mice after timed breeding revealed that viable ROMO1$^{-/-}$ embryos were not found after embryonic day (E) 8.5 (Fig. 1 D, E). We confirmed dose-dependent loss of ROMO1 mRNA in heterozygous and homozygous mice (Figure 1F). Expression of the Nfs1 gene, that overlaps with ROMO1 but is transcribed from the opposite strand, was normal by RT-PCR (Figure 1G). Thus, we conclude that our knockout strategy specifically targeted ROMO1, and that ROMO1 is essential for embryonic development in mice. The timing of *ROMO1*$^{-/-}$ embryonic lethality is earlier than that of mice lacking *Mfn1*, *Mfn2*, or *Opa1*, which like ROMO1, are necessary for mitochondrial fusion [1,21-23]. ATP levels in control and ROMO1 silenced U2OS cells were unchanged, indicating loss of ROMO1 is not required for maintenance of steady state cellular energy levels in this context

(Supplementary Figure 1). This suggests that, in addition to regulation of mitochondrial fusion [1], ROMO1 may serve a more primordial role essential to embryonic development in mice.

ROMO1 is required for energy coupling in the pancreatic β cell

The pancreatic β cell synthesizes and secretes insulin in response to feeding cues and is essential for glucose homeostasis. Death or dysfunction of β cells is a central causal feature in diabetes [24]. Insulin secretion is an energetically demanding process that is accompanied by significant ROS production that must be controlled by cellular reductive systems [25]; uncontrolled ROS production is a hallmark of Type 2 diabetes [26]. To test if ROMO1 is required to regulate ROS and cellular energetics *in vivo*, we generated a pancreatic β cell-specific knockout of ROMO1 using a *Pdx1-ER^{Tam}-Cre* transgenic line [19,20], which expresses Cre recombinase in the pancreatic β cell compartment (Fig. 2A). By breeding *ROMO1$^{+/flox}$* mice to *ROMO1$^{flox/+}$:Pdx1- CreER^{Tam}* mice, we generated *ROMO1$^{flox/flox}$:Pdx1-CreER^{Tam}*mice, that in the presence of tamoxifen produce the nonsense ROMO1 transcript in adult β cells which is then eliminated. We refer to these mice as ROMO1 adult β cell knockout (RABKO) mice. As controls, we used *ROMO1$^{+/+}$:Pdx1-CreER^{Tam}* mice, which are phenotypically wild type (referred to below as WT). RABKO mice were born at normal frequencies and had body weights indistinguishable from littermate controls (not shown). Western blot revealed ~70% reduction of ROMO1 protein in islets isolated from RABKO mice, consistent with the relative fraction of β cells in islets, as well as unchanged levels of ROMO1 in the cortex and hypothalamus (Figure 2B), consistent with our previous work with the *Pdx1-CreER^{Tam}* transgene [19,20]. Islet morphology was normal in RABKO mice, and insulin staining

revealed an trend towards smaller islets in RABKO mice (Figure 2C). Immunostaining for insulin and glucagon confirmed that alpha and delta cell populations were unaffected (Figure 2D).

Male and female RABKO mice at 10 weeks of age were normoglycemic after an overnight fast but showed elevated blood glucose after 1 hour of refeeding, with RABKO males showing more pronounced hyperglycemia than females (Figure 3A). Heterozygous males and female mice were normal. Male but not female RABKO mice showed lower plasma insulin after 1 hour of refeeding (Figure 3B), and when challenged with an IP glucose bolus, male but not female mice were glucose intolerant (Figure 3C) and had significantly reduced plasma insulin levels (Figure 3D). As the animals aged, female mice showed mild glucose intolerance (not shown).

We next performed an arginine tolerance test that showed that male RABKO mice failed to mount an acute insulin secretory response to this amino acid (Figure 3E). Static insulin secretion assays demonstrated that both glucose-stimulated and depolarization-induced insulin secretion (following KCl treatment) was reduced by 50% in male RABKO islets compared to WT islets (Figure 3F), despite a normal insulin content (Figure 3G). Islets isolated from female RABKO islets were phenotypically normal, indicative of a sex-specific defect in glucose coupling and/or granule recruitment post-membrane depolarization. Taken together, the data indicate that ROMO1 in the β cell is required for nutrient coupling and maintenance of euglycemia in male mice.

Cristae defects and loss of SRC in RABKO β cells

We previously reported altered cristae in cultured cells silenced for ROMO1 by RNA interference[1]. To determine whether this effect also occurs in primary cells carrying a ROMO1 deletion, we analyzed mitochondrial ultrastructure in male WT and RABKO β cells. In WT β cells, mitochondria appeared as long tubular structures with ordered cristae (Figure 4A). In contrast, mitochondria in RABKO β cells displayed fewer cristae, some of which were floating without a clear connection to the IMM, as well as rod-like structures (not shown) seen in mitochondria defective in membrane fusion [27-29]. Furthermore, RABKO mitochondria were visibly swollen, and insulin granules in RABKO mice were less electron dense and showed rod-shaped insulin crystals, consistent with immature or pathological Zn^{2+}-dependent packing of insulin [30]. To determine if these ultrastructural changes in cells lacking ROMO1 resulted in loss of respiratory activity, we compared oxygen consumption rates in male WT and RABKO islets. While loss of ROMO1 did not affect the basal respiration rate (with complex I fuel glucose present) or respiration in response to complex IV fuels TMPD and ascorbate, the maximal oxygen consumption rate following treatment with the uncoupling agent FCCP was reduced (Figure 4B), consistent with our previous work [1]. Spare respiratory capacity (SRC) was reduced by 50% in RABKO islet cells (Figure 4C). A similar loss of SRC was seen following silencing of ROMO1 in isolated male human islets (Figure 4D). We next asked if this loss of SRC was a consequence of mitochondrial fragmentation that occurs in the absence of ROMO1. Interestingly, in contrast to cells lacking ROMO1, SRC was minimally affected by fragmentation induced by silencing the GTPases that catalyze fusion of the outer (MFN1/2) or inner (OPA1) mitochondrial membranes in U2OS cells (Figure 4E-F). We conclude that the loss of SRC in cells lacking ROMO1 is not due to a defect in membrane fusion per se, but instead results from a bioenergetic defect in cells lacking ROMO1. Staining U2OS cells

silenced for ROMO1 with the potentiometric dye TMRE revealed that IMM potential after treatment with FCCP or oligomycin was not altered by the absence of ROMO1, indicating that the loss of SRC was not due to increased potential across the IMM (Supplementary Figure 2). We next performed proteinase K protection assays with mitochondria isolated from U2OS cells to confirm ROMO1's subcellular localization and possible orientation in the IMM. Western blots for ROMO1 using a commercial antibody with an N-terminal epitope (Origene) and another we prepared (Covance) with an epitope in an interhelix sequence, revealed that ROMO1 is localized to the IMM (Figure 4G), and given the second predicted helical sequence (TM2, [1]), we predict a hairpin loop orientation (red box in Figure 4H).

Discussion

In this study we used a null allele of *ROMO1* to generate a mammalian model of defective mitochondrial spare respiratory capacity and demonstrate that ROMO1 is essential for early embryonic development in mice. Because silencing ROMO1 does not severely reduce total intracellular ATP in cultured cells [1], we suggest that IMM fusion in this setting is not essential for net ATP generation under basal conditions. Using a conditional allele of *ROMO1*, we showed that ROMO1 is required for maintenance of euglycemia by facilitating glucose coupling in the pancreatic β cell. That there are metabolites in addition to glucose-derived pyruvate required for efficient coupling of glucose to insulin output has been appreciated for over 20 years, with NADH generated during glycolysis being an essential cofactor in eliciting insulin secretion [31]. Our data demonstrate that ROMO1 is a key regulator of mitochondrial bioenergetics and spare respiratory activity.

While Richter and colleagues observed a global loss of complex IV in ROMO1 null cells [17], complex IV-dependent respiration was normal in RABKO islets. Instead, RABKO islets showed a loss of spare respiratory capacity (SRC), consistent with our previous work [1]. SRC is essential for mitochondria to generate ATP by oxidative phosphorylation under increased demand [32], and loss of SRC is a hallmark of aging cells [33]. Under normal conditions, the majority of electrons from NADH enter the electron transport chain at complex I, with the remaining entering an auxiliary path at complex II, which is also known as succinate oxidoreductase or succinate dehydrogenase (SDH) of the TCA cycle [34]. Recent work has implicated mitochondrial complex II as a source of SRC, as under stress, mitochondria increase their respiratory output by increasing electron flow through this auxiliary path [32]. Consistent with this, complex II is critical both in development and in aging, where loss of complex II respiration results in succinate accumulation and ROS generation, and drives age-related diseases, including diabetes [26]. We speculate that reducing equivalents generated at complex II, not through the classic I-III-IV pathway, are essential for SRC and glucose stimulated insulin secretion, for which there is precedence [35].

Mitochondria lacking ROMO1 are swollen and show disorganized and sometimes floating cristae. How does loss of ROMO1 lead to mitochondrial morphology changes? Membrane curvature associated with cristae junctions is thought to be established by dimerization of ATP synthase (complex V) and of the MICOS complex, which establishes a boundary between inner membrane that are dedicated to cristae vs. non-cristae regions [36,37]. ROMO1 coprecipitates with mitofilin [1], the core component of the MICOS complex, and with OPA1, the GTPase required for IMM fusion. In the absence of ROMO1, OPA1 processing is abnormal [1], and likely contributes to dysfunctional IMM dynamics. Our data demonstrating loss of SRC in the absence of ROMO1 prompt a model

whereby loss of bioenergetic activity at complex II lies upstream of dysfunction in MICOS and OPA1. Interestingly, complex II, unlike complexes I, III, IV and V, is clustered near cristae junctions and does not line the entire length of cristae [38].

Our biochemical data confirm that ROMO1 is localized to the IMM, and together with our bioinformatic analysis predicting that ROMO1 would form two amphipathic helixes [1], we predict that ROMO1 forms a hairpin structure in the IMM. Such a conformation would bring highly conserved Cys residues at positions 15 and 79 into close apposition in the IMS, with the resulting 10 amino acid loop residing in the matrix. Of note, assembly of three ROMO1 molecules in such a confirmation would resemble carriers of the Solute Ligand Carrier family [39], and Yoo and colleagues demonstrated that ROMO1 can act as a nonselective monovalent cation channel [18]. It remains tempting to speculate that ROMO1 may govern bioenergetic activity by contributing to ion flux across the IMM.

We show that male mouse islets lacking ROMO1 show defects in insulin secretion in response to glucose and depolarization, yet females are unaffected. Sex differences in homeostatic physiology are being recognized as the basis for differences in both pathology and treatment responses in specific brain regions and in stress-based pathophysiology, and this is true for insulin secretion in both rodent models and humans [40,41]. Significant reductions in insulin secretion are observed with aging in humans, but only in males [42], an effect that may be attributed to sex-specific genomic methylation patterns [43]. Our data raise the possibility that β cells in males uniquely rely on SRC under normal conditions to fulfill an insulin secretory response. As SRC is lost in aging, this may in part explain the preferential loss of insulin secretion in aging males. Taken together, our data

indicate that strategies to promote ROMO1 activity would enhance glucose coupling, insulin secretion and glucose tolerance in males.

Acknowledgements LW, CI, and ACHN performed experiments and edited manuscript. CR and SPY performed experiments. RAS designed the project and wrote the manuscript. We would like to acknowledge Lindsey Fiddes at the University of Toronto Microscopy Imaging Lab for EM sample processing and imaging and Judy Cathcart University Health Network, Division of Biophysics and Bioimaging for imaging of stained pancreatic sections. The authors declare no conflict of interest. The project was supported by Canadian Institutes of Health Research Project Grant 142352 to RAS. RAS is the guarantor of this work and, as such, had full access to all the data in the study and takes responsibility for the integrity of the data and the accuracy of the data analysis. Some of the data in the manuscript has been presented at scientific meetings.

Figure Legends

1. Early embryonic lethality in ROMO1 knockout mice. A. Knockout strategy. Position of overlapping antisense gene Nfs1 shown. B. Genotyping of pups carrying KO allele. C. Live birth genotypes. D. Micrograph of embryos dissected at e10.5 then genotyped. KO embryo shown. E. Whole mount micrographs of WT and KO embryo at e8.5 showing early lethality of embryos

lacking ROMO1. F. RT-PCR analysis of ROMO1 and G. Nfs1 levels from WT, HET and cardiac ROMO1 KO (to be described elsewhere), demonstrating Nfs1 expression after Cre-mediated recombination is unperturbed.

2. Generation of ROMO1 adult β cell knockout (RABKO) mice. A. Conditional ROMO1 adult β cell knockout schematic and genotyping analysis of DNA from Cre+ animals carrying ROMO1 +/+ or fl/fl alleles, showing recombination only in fl/fl Cre+ islets and no other tissue. B. Western blot of ROMO1 in cortex, hypothalamus and islets of WT and RABKO mice showing loss of ROMO1 only in the islet samples. Loading control for the samples is ERK2. C. (top) H+E staining of pancreatic sections from WT (+/+, Cre+) and RABKO (fl/fl, Cre+) mice. (bottom) Insulin staining in pancreatic sections. D. Immunofluorescent imaging of insulin (green) and glucagon (red) with DAPI counterstain on pancreatic sections from WT or RABKO mice showing normal islet morphology.

Figure 3. Glucose intolerance in RABKO mice. A. Fasted and 2-hour refed blood glucose in 10-week old male mice (left) and female mice (right). B. Plasma insulin levels from male and female mice in A. C. IPGTT assay in WT and RABKO 10-week old male and female mice. D. Plasma insulin levels in WT (black bars) and RABKO (white bars) 10-week old male and female mice during IPGTT glucose challenge. E. Plasma insulin levels in WT and RABKO male mice after arginine injection. F. Static GSIS assay with islets isolated from 10-week old male and female WT and RABKO mice incubated 2.8 mM glucose prior to stimulation with 16.7 mM glucose or 45 mM KCl to depolarize the cells. G. Insulin content in islets from WT and RABKO mice.

Figure 4. ROMO1 is required for spare respiratory capacity. A. Electron micrographs showing mitochondrial morphology and fewer cristae in 10-week old RABKO mice. RABKO β cells contain more immature insulin granules (grey centres). Images on right are 2X magnification of region highlighted by white box on left. Scale bars = 500 nM. B. Seahorse assay showing oxygen consumption in dissociated islet cells isolated from male WT (black line) and RABKO mice (red line). Treatment with oligomycin (O), FCCP (F), rotenone/Antimycin A (R/A), and complex IV fuels TMPD and ascorbate (ASC) are indicated. C. Barplot of spare respiratory capacity (SRC) from panel B. D. Seahorse assay showing loss of SRC in male human β cells following ROMO1 silencing. Treatment with oligomycin (O), FCCP (F), and rotenone/Antimycin A (R/A) are indicated. Western blot showing the ROMO1 knockdown is inset. E. Oxygen consumption in U2OS cells silenced for OPA1, MFN1+2, or ROMO1. Treatment with oligomycin (O), FCCP (F), and rotenone/Antimycin A (R/A) are indicated. F. Western blots showing levels of proteins silenced in E. G**.** Sodium carbonate extraction and Proteinase K (PK) assay shows ROMO1 is an integral membrane protein. Cytosolic protein extracts were loaded as a control. TOMM20 was digested by PK prior to osmotic shock, confirming its OMM localization. N-terminal epitope ROMO1 Ab (Origene) showed that ROMO1 behaves like OPA1 (an IMM protein). A ROMO1 antibody (Covance) we prepared that recognizes the inter-helix loop region showed a PK digestion pattern similar to SOD2, suggesting that if the hairpin model is correct, that the loop faces the matrix. H. (Top) Schematic of ROMO1 to illustrate domain structure and location of antibody epitopes for model shown. TM1 was previously predicted by bioinformatic analyses [44], TM2 is a putative TM domain predicted by our analysis [1] and confirmed by [18]. (Bottom) Schematic of possible ROMO1 orientations in the IMM. Red crosses indicate orientation that were ruled out using PK data; options 4 and 5 are still formally possible.

Supplementary Figure Legends

1. ATP levels in U2OS cells transfected with control non-targeting (CON) or ROMO1 RNAi duplexes were determined by mass spectrometry.
2. Mitochondrial membrane potential measurements following treatment with proton gradient uncoupler FCCP or ATP synthase inhibitor oligomycin are unchanged in ROMO1-silenced U2OS cells. Data were normalized to untreated siCON cells in each graph.

References

1 Norton, M., Ng, A. C., Baird, S., Dumoulin, A., Shutt, T., Mah, N., Andrade-Navarro, M. A., McBride, H. M. & Screaton, R. A. ROMO1 Is an Essential Redox-Dependent Regulator of Mitochondrial Dynamics. *Science signaling* **7**, ra10, doi:10.1126/scisignal.2004374 (2014).

2 Brand, M. D. & Nicholls, D. G. Assessing mitochondrial dysfunction in cells. *Biochem J* **435**, 297-312, doi:10.1042/BJ20110162 (2011).

3 Giorgi, C., Marchi, S. & Pinton, P. The machineries, regulation and cellular functions of mitochondrial calcium. *Nat Rev Mol Cell Biol* **19**, 713-730, doi:10.1038/s41580-018-0052-8 (2018).

4 Rizzuto, R., De Stefani, D., Raffaello, A. & Mammucari, C. Mitochondria as sensors and regulators of calcium signalling. *Nat Rev Mol Cell Biol* **13**, 566-578, doi:10.1038/nrm3412 (2012).

5 Jang, J. Y., Blum, A., Liu, J. & Finkel, T. The role of mitochondria in aging. *J Clin Invest* **128**, 3662-3670, doi:10.1172/JCI120842 (2018).

6 Tian, R., Colucci, W. S., Arany, Z., Bachschmid, M. M., Ballinger, S. W., Boudina, S., Bruce, J. E., Busija, D. W., Dikalov, S., Dorn, G. W., II, Galis, Z. S., Gottlieb, R. A., Kelly, D. P., Kitsis, R. N., Kohr, M. J., Levy, D., Lewandowski, E. D., McClung, J. M., Mochly-Rosen, D., O'Brien, K. D., O'Rourke, B., Park, J. Y., Ping, P., Sack, M. N., Sheu, S. S., Shi, Y., Shiva, S., Wallace, D. C., Weiss, R. G., Vernon, H. J., Wong, R. & Schwartz Longacre, L. Unlocking the Secrets of Mitochondria in the Cardiovascular

System: Path to a Cure in Heart Failure-A Report from the 2018 National Heart, Lung, and Blood Institute Workshop. *Circulation* **140**, 1205-1216, doi:10.1161/CIRCULATIONAHA.119.040551 (2019).

7 Nahapetyan, H., Moulis, M., Grousset, E., Faccini, J., Grazide, M. H., Mucher, E., Elbaz, M., Martinet, W. & Vindis, C. Altered mitochondrial quality control in Atg7-deficient VSMCs promotes enhanced apoptosis and is linked to unstable atherosclerotic plaque phenotype. *Cell death & disease* **10**, 119, doi:10.1038/s41419-019-1400-0 (2019).

8 Yu, E. P. K., Reinhold, J., Yu, H., Starks, L., Uryga, A. K., Foote, K., Finigan, A., Figg, N., Pung, Y. F., Logan, A., Murphy, M. P. & Bennett, M. Mitochondrial Respiration Is Reduced in Atherosclerosis, Promoting Necrotic Core Formation and Reducing Relative Fibrous Cap Thickness. *Arterioscler Thromb Vasc Biol* **37**, 2322-2332, doi:10.1161/ATVBAHA.117.310042 (2017).

9 Zuo, L., Prather, E. R., Stetskiv, M., Garrison, D. E., Meade, J. R., Peace, T. I. & Zhou, T. Inflammaging and Oxidative Stress in Human Diseases: From Molecular Mechanisms to Novel Treatments. *Int J Mol Sci* **20**, doi:10.3390/ijms20184472 (2019).

10 Dai, W. & Jiang, L. Dysregulated Mitochondrial Dynamics and Metabolism in Obesity, Diabetes, and Cancer. *Front Endocrinol (Lausanne)* **10**, 570, doi:10.3389/fendo.2019.00570 (2019).

11 Spinelli, J. B. & Haigis, M. C. The multifaceted contributions of mitochondria to cellular metabolism. *Nat Cell Biol* **20**, 745-754, doi:10.1038/s41556-018-0124-1 (2018).

12 Shi, Y. A structural view of mitochondria-mediated apoptosis. *Nat Struct Biol* **8**, 394-401, doi:10.1038/87548 (2001).

13 Chung, Y. M., Kim, J. S. & Yoo, Y. D. A novel protein, Romo1, induces ROS production in the mitochondria. *Biochem Biophys Res Commun* **347**, 649-655, doi:10.1016/j.bbrc.2006.06.140 (2006).

14 Na, A. R., Chung, Y. M., Lee, S. B., Park, S. H., Lee, M. S. & Yoo, Y. D. A critical role for Romo1-derived ROS in cell proliferation. *Biochem Biophys Res Commun* **369**, 672-678, doi:10.1016/j.bbrc.2008.02.098 (2008).

15 Shin, J. A., Chung, J. S., Cho, S. H., Kim, H. J. & Yoo, Y. D. Romo1 expression contributes to oxidative stress-induced death of lung epithelial cells. *Biochem Biophys Res Commun*, doi:10.1016/j.bbrc.2013.07.012 (2013).

16 Wu, H., Gu, Y. H., Wei, L., Guo, T. K., Zhao, Y., Su, G., Li, J. & Xie, X. D. Association of Romo1 gene genetic polymorphisms with risk of gastric cancer in northwestern Chinese population. *Pathol Oncol Res* **21**, 581-587, doi:10.1007/s12253-014-9858-7 (2015).

17 Richter, F., Dennerlein, S., Nikolov, M., Jans, D. C., Naumenko, N., Aich, A., MacVicar, T., Linden, A., Jakobs, S., Urlaub, H., Langer, T. & Rehling, P. ROMO1 is a constituent of the human presequence translocase required for YME1L protease import. *J Cell Biol* **218**, 598-614, doi:10.1083/jcb.201806093 (2019).

18 Lee, G. Y., You, D. G., Lee, H. R., Hwang, S. W., Lee, C. J. & Yoo, Y. D. Romo1 is a mitochondrial nonselective cation channel with viroporin-like characteristics. *J Cell Biol* **217**, 2059-2071, doi:10.1083/jcb.201709001 (2018).

19 Fu, A., Ng, A. C., Depatie, C., Wijesekara, N., He, Y., Wang, G. S., Bardeesy, N., Scott, F. W., Touyz, R. M., Wheeler, M. B. & Screaton, R. A. Loss of Lkb1 in adult beta cells increases beta cell mass and enhances glucose tolerance in mice. *Cell Metab* **10**, 285-295 (2009).

20 Sakamaki, J., Fu, A., Reeks, C., Baird, S., Depatie, C., Al Azzabi, M., Bardeesy, N., Gingras, A. C., Yee, S. P. & Screaton, R. A. Role of the SIK2-p35-PJA2 complex in pancreatic beta-cell functional compensation. *Nat Cell Biol* **16**, 234-244, doi:10.1038/ncb2919 (2014).

21 Chen, H., Detmer, S. A., Ewald, A. J., Griffin, E. E., Fraser, S. E. & Chan, D. C. Mitofusins Mfn1 and Mfn2 coordinately regulate mitochondrial fusion and are essential for embryonic development. *J Cell Biol* **160**, 189-200, doi:10.1083/jcb.200211046 (2003).

22 Alavi, M. V., Bette, S., Schimpf, S., Schuettauf, F., Schraermeyer, U., Wehrl, H. F., Ruttiger, L., Beck, S. C., Tonagel, F., Pichler, B. J., Knipper, M., Peters, T., Laufs, J. & Wissinger, B. A splice site mutation in the murine Opa1 gene features pathology of autosomal dominant optic atrophy. *Brain* **130**, 1029-1042, doi:10.1093/brain/awm005 (2007).

23 Davies, V. J., Hollins, A. J., Piechota, M. J., Yip, W., Davies, J. R., White, K. E., Nicols, P. P., Boulton, M. E. & Votruba, M. Opa1 deficiency in a mouse model of autosomal dominant optic atrophy impairs mitochondrial morphology, optic nerve structure and visual function. *Hum Mol Genet* **16**, 1307-1318, doi:ddm079 [pii] 10.1093/hmg/ddm079 (2007).

24 Eizirik, D. L. & Darville, M. I. beta-cell apoptosis and defense mechanisms: lessons from type 1 diabetes. *Diabetes* **50 Suppl 1**, S64-69 (2001).

25 Newsholme, P., Keane, K. N., Carlessi, R. & Cruzat, V. Oxidative stress pathways in pancreatic beta-cells and insulin-sensitive cells and tissues: importance to cell metabolism, function, and dysfunction. *Am J Physiol Cell Physiol* **317**, C420-C433, doi:10.1152/ajpcell.00141.2019 (2019).

26 Green, K., Brand, M. D. & Murphy, M. P. Prevention of mitochondrial oxidative damage as a therapeutic strategy in diabetes. *Diabetes* **53 Suppl 1**, S110-118, doi:10.2337/diabetes.53.2007.s110 (2004).

27 Olichon, A., Baricault, L., Gas, N., Guillou, E., Valette, A., Belenguer, P. & Lenaers, G. Loss of OPA1 perturbates the mitochondrial inner membrane structure and integrity, leading to cytochrome c release and apoptosis. *J Biol Chem* **278**, 7743-7746, doi:10.1074/jbc.C200677200 (2003).

28 Griparic, L., van der Wel, N. N., Orozco, I. J., Peters, P. J. & van der Bliek, A. M. Loss of the intermembrane space protein Mgm1/OPA1 induces swelling and localized constrictions along the lengths of mitochondria. *J Biol Chem* **279**, 18792-18798, doi:10.1074/jbc.M400920200 (2004).

29 Chen, H., Chomyn, A. & Chan, D. C. Disruption of fusion results in mitochondrial heterogeneity and dysfunction. *J Biol Chem* **280**, 26185-26192 (2005).

30 Wijesekara, N., Dai, F. F., Hardy, A. B., Giglou, P. R., Bhattacharjee, A., Koshkin, V., Chimienti, F., Gaisano, H. Y., Rutter, G. A. & Wheeler, M. B. Beta cell-specific Znt8 deletion in mice causes marked defects in insulin processing, crystallisation and secretion. *Diabetologia* **53**, 1656-1668, doi:10.1007/s00125-010-1733-9 (2010).

31 Eto, K., Tsubamoto, Y., Terauchi, Y., Sugiyama, T., Kishimoto, T., Takahashi, N., Yamauchi, N., Kubota, N., Murayama, S., Aizawa, T., Akanuma, Y., Aizawa, S., Kasai, H., Yazaki, Y. & Kadowaki, T. Role of NADH shuttle system in glucose-induced activation of mitochondrial metabolism and insulin secretion. *Science* **283**, 981-985, doi:10.1126/science.283.5404.981 (1999).

32 Pfleger, J., He, M. & Abdellatif, M. Mitochondrial complex II is a source of the reserve respiratory capacity that is regulated by metabolic sensors and promotes cell survival. *Cell death & disease* **6**, e1835, doi:10.1038/cddis.2015.202 (2015).

33 Pence, B. D. & Yarbro, J. R. Aging impairs mitochondrial respiratory capacity in classical monocytes. *Experimental gerontology* **108**, 112-117, doi:10.1016/j.exger.2018.04.008 (2018).

34 Maio, N., Ghezzi, D., Verrigni, D., Rizza, T., Bertini, E., Martinelli, D., Zeviani, M., Singh, A., Carrozzo, R. & Rouault, T. A. Disease-Causing SDHAF1 Mutations Impair Transfer of Fe-S Clusters to SDHB. *Cell Metab* **23**, 292-302, doi:10.1016/j.cmet.2015.12.005 (2016).

35 Edalat, A., Schulte-Mecklenbeck, P., Bauer, C., Undank, S., Krippeit-Drews, P., Drews, G. & Dufer, M. Mitochondrial succinate dehydrogenase is involved in stimulus-secretion coupling and endogenous ROS formation in murine beta cells. *Diabetologia* **58**, 1532-1541, doi:10.1007/s00125-015-3577-9 (2015).

36 Cogliati, S., Enriquez, J. A. & Scorrano, L. Mitochondrial Cristae: Where Beauty Meets Functionality. *Trends Biochem Sci* **41**, 261-273, doi:10.1016/j.tibs.2016.01.001 (2016).

37 Kozjak-Pavlovic, V. The MICOS complex of human mitochondria. *Cell Tissue Res* **367**, 83-93, doi:10.1007/s00441-016-2433-7 (2017).

38 Wilkens, V., Kohl, W. & Busch, K. Restricted diffusion of OXPHOS complexes in dynamic mitochondria delays their exchange between cristae and engenders a transitory mosaic distribution. *J Cell Sci* **126**, 103-116, doi:10.1242/jcs.108852 (2013).

39 Bai, X., Moraes, T. F. & Reithmeier, R. A. F. Structural biology of solute carrier (SLC) membrane transport proteins. *Mol Membr Biol* **34**, 1-32, doi:10.1080/09687688.2018.1448123 (2017).

40 Li, T., Jiao, W., Li, W. & Li, H. Sex effect on insulin secretion and mitochondrial function in pancreatic beta cells of elderly Wistar rats. *Endocr Res* **41**, 167-179, doi:10.3109/07435800.2015.1124437 (2016).

41 Basu, R., Dalla Man, C., Campioni, M., Basu, A., Klee, G., Toffolo, G., Cobelli, C. & Rizza, R. A. Effects of age and sex on postprandial glucose metabolism: differences in glucose turnover, insulin secretion, insulin action, and hepatic insulin extraction. *Diabetes* **55**, 2001-2014, doi:10.2337/db05-1692 (2006).

42 Arrojo e Drigo, R., Erikson, G., Tyagi, S., Capitanio, J., Lyon, J., Spigelman, A. F., Bautista, A., Manning Fox, J. E., Shokhirev, M., MacDonald, P. E. & Hetzer, M. W. Aging of human endocrine pancreatic cell types is heterogeneous and sex-specific. *bioRxiv*, 729541, doi:10.1101/729541 (2019).

43 Hall, E., Volkov, P., Dayeh, T., Esguerra, J. L., Salo, S., Eliasson, L., Ronn, T., Bacos, K. & Ling, C. Sex differences in the genome-wide DNA methylation pattern and impact on gene expression, microRNA levels and insulin secretion in human pancreatic islets. *Genome Biol* **15**, 522, doi:10.1186/s13059-014-0522-z (2014).

44 Zhao, J., Liu, T., Jin, S. B., Tomilin, N., Castro, J., Shupliakov, O., Lendahl, U. & Nister, M. The novel conserved mitochondrial inner-membrane protein MTGM regulates mitochondrial morphology and cell proliferation. *J Cell Sci* **122**, 2252-2262, doi:10.1242/jcs.038513 (2009).

Figure 1

A

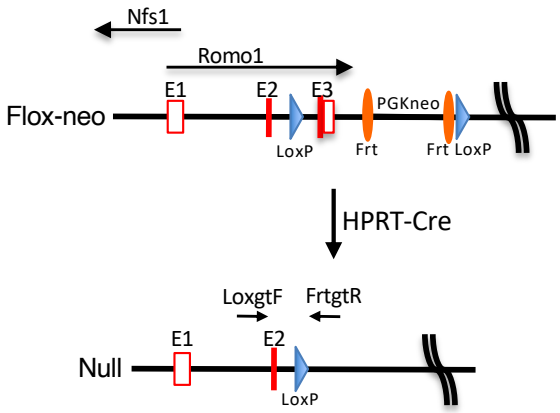

B

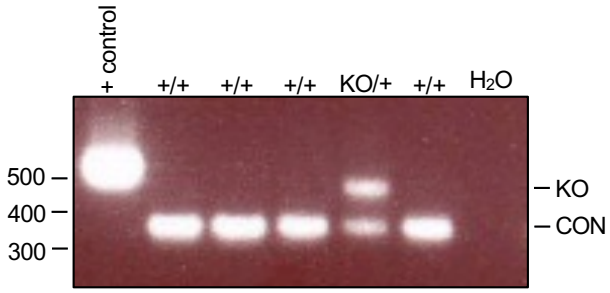

C

	+/+	+/-	-/-
Neonates observed	24/69	45/69	0/69
Neonates expected	17.25	34.5	17.25
% of total	35	65	0
P < 0.00001			

D

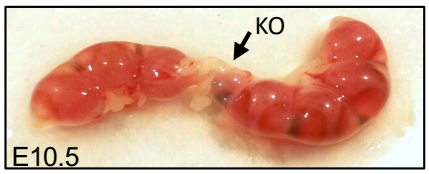

E

F

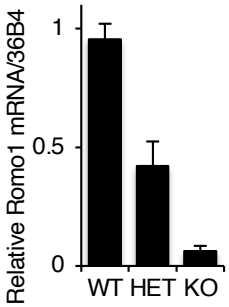

G

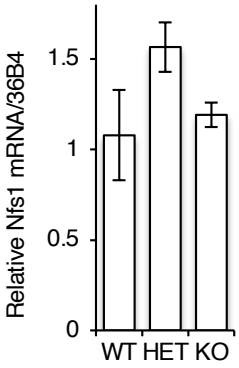

Figure 2

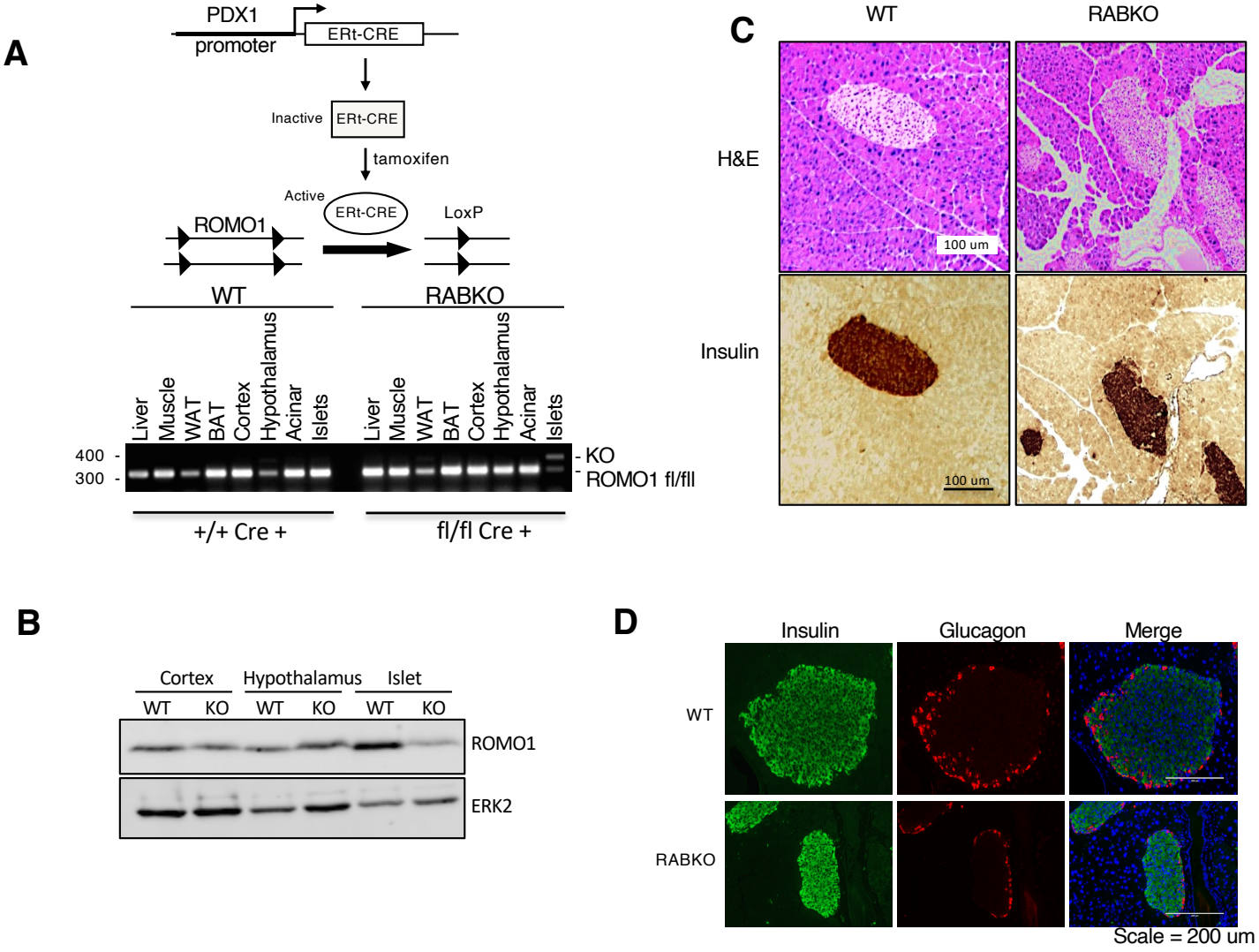

Figure 3

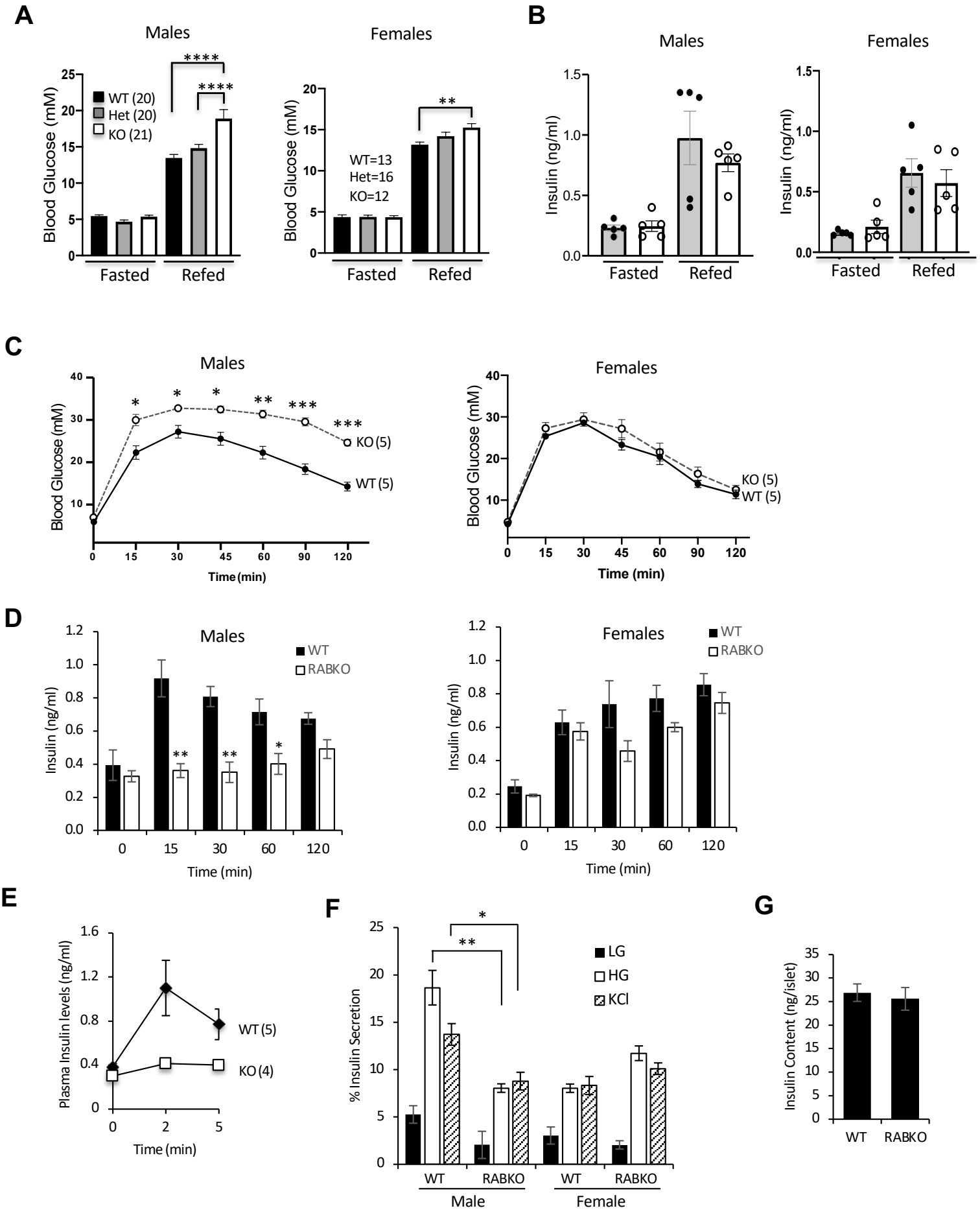

Figure 4

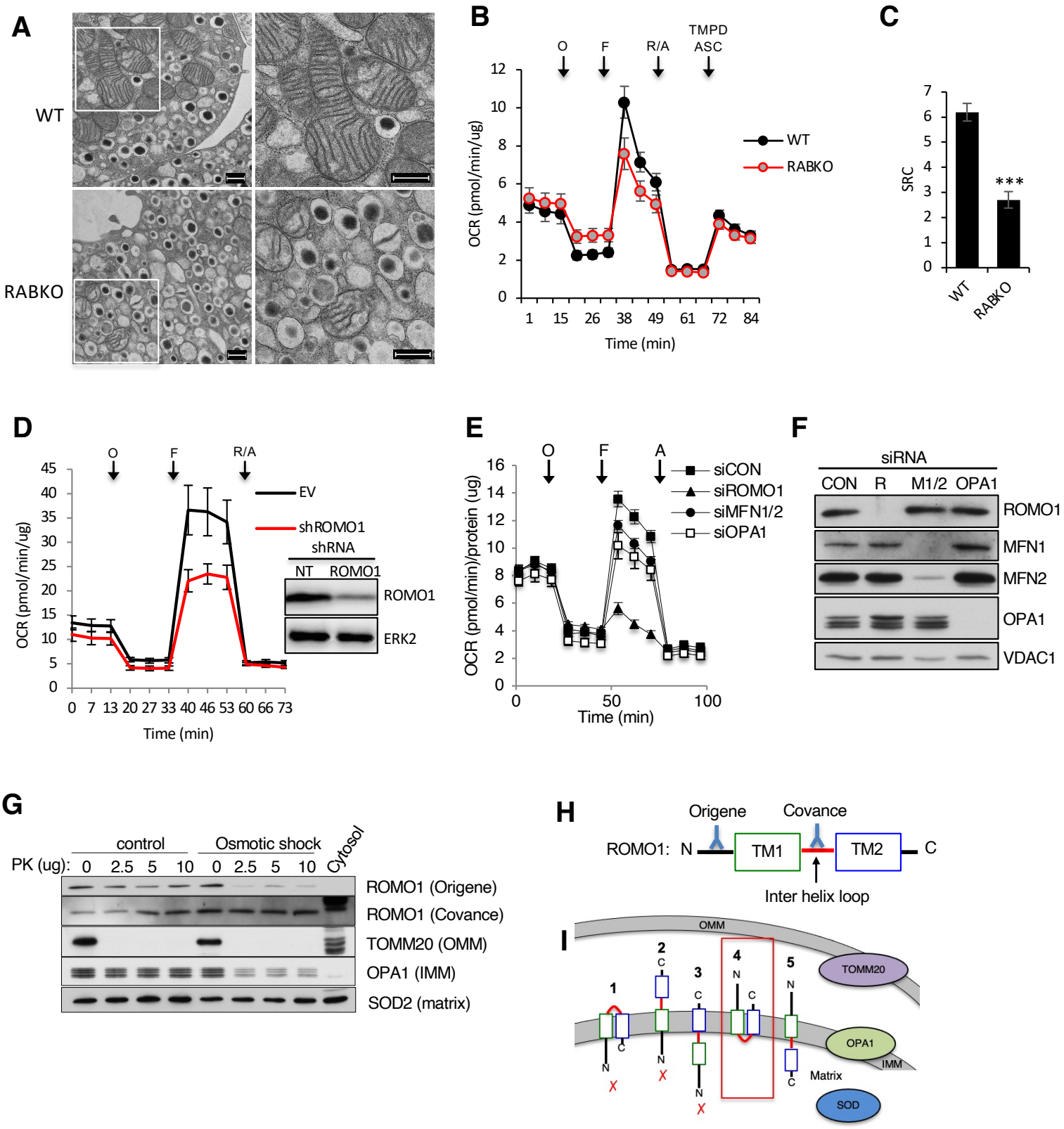

Supplementary Figures

1

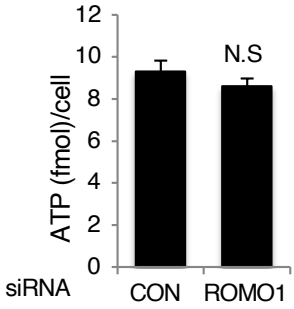

2